Hydrodeoxygenation of Guaiacol over Carbon-Supported Metal Catalysts

Jie Chang,* Tanate Danuthai, Silvia Dewiyanti, Chuan Wang, and Armando Borgna*[a]

Catalytic bio-oil upgrading to produce renewable fuels has attracted increasing attention in response to the decreasing oil reserves and the increased fuel demand worldwide. Herein, the catalytic hydrodeoxygenation (HDO) of guaiacol with carbon-supported non-sulfided metal catalysts was investigated. Catalytic tests were performed at 4.0 MPa and temperatures ranging from 623 to 673 K. Both Ru/C and Mo/C catalysts showed promising catalytic performance in HDO. The selectivity to benzene was 69.5 and 83.5% at 653 K over Ru/C and 10Mo/C catalysts, respectively. Phenol, with a selectivity as high as 76.5%, was observed mainly on 1Mo/C. However, the reaction pathway over both catalysts is different. Over the Ru/C catalyst, the O–CH_3 bond was cleaved to form the primary intermediate catechol, whereas only traces of catechol were detected over Mo/C catalysts. In addition, two types of active sites were detected over Mo samples after reduction in H_2 at 973 K. Catalytic studies showed that the demethoxylation of guaiacol is performed over residual MoO_x sites with high selectivity to phenol whereas the consecutive HDO of phenol is performed over molybdenum carbide species, which is widely available only on the 10Mo/C sample. Different deactivation patterns were also observed over Ru/C and Mo/C catalysts.

Introduction

Bio-oils produced from the fast pyrolysis of lignocellulosic biomass contain complex mixtures of reactive oxygenate compounds, such as carboxylic acids, aldehydes, ketones, furans, sugars, carbohydrates and water.[1] The presence of these compounds in bio-oils leads to the undesired fuel properties, such as instability, high acidity, high viscosity and poor heating value.[2] Therefore, the removal of oxygenate functional groups is an important step in obtaining high-quality fuels from the low-cost bio-oils.[3] Various processes such as cracking and hydrodeoxygenation (HDO) have been proposed to convert bio-oils into alternative liquid fuels.[4]

Owing to the thermal instability of bio-oil, a two-stage upgrading strategy was proposed. In the first stage the stabilisation of active organic compounds, such as ketones, aldehydes and some acids, is performed under mild temperatures, whereas in the second stage a deep HDO of stabilised bio-oil is performed using higher temperatures. In this way, the yield loss and coking can be inhibited effectively.

The HDO of bio-oil is generally performed by using a hydrotreating process under high pressure. Conventional hydrodesulfurization catalysts, particularly sulfided NiMo and CoMo catalysts, have been used in this application.[5] These catalysts can provide a good HDO activity and conversions up to 95%, together with a significant bio-oil yield at bench scale.[6] However, their industrial application seems to be hindered by the gradual sulfur removal during the long-term operation because the sulfur content in bio-oil is quite low.[7] Co-feeding of H_2S can regenerate the sulfide sites and therefore stabilise the catalyst. However, the resulting fuels are contaminated by sulfur, which loses the advantage of sulfur-free fuels. Furthermore, the presence of water and carboxylic acid in bio-oil can result in the instability of alumina supports and serious coke formation.[8,9] Thus, significant efforts have been made to develop carbon-supported non-sulfided catalysts for bio-oil upgrading.[10]

Transition metal-based catalysts, particularly noble metal catalysts, can also be used in HDO reactions.[11] Heeres et al.[11a] reported the valuable screening results for noble metal and sulfided Mo-based catalysts in the bio-oil HDO reaction. It was found that the carbon-supported noble metal catalysts have better performance than the latter. Particularly, the Ru/C catalyst is the most promising candidate for bio-oil upgrading in terms of oil yields, deoxygenation activity and hydrogen consumption. Although the Pd/C catalyst provided higher oil yields than the Ru/C catalyst, the higher hydrogen consumption and higher oxygen content in the products are the major drawbacks. However, char and heavily viscous products formed in the batch reactor set-up from the raw bio-oil hindered the quantitative analysis, and thus the understanding of the reaction mechanisms.

Molybdenum carbides and oxycarbides were found to be active in hydrotreatment and HDO reactions.[12] These materials have electronic and catalytic properties similar to those of the noble metals, but are more resistant to poisons such as sulfur and to sintering; thus, they are potential substitutes for expensive and scarce noble metals. However, there are few reports

[a] *Dr. J. Chang, Dr. T. Danuthai, S. Dewiyanti, Dr. C. Wang, Dr. A. Borgna*
Heterogeneous Catalysis Department
Institute of Chemical and Engineering Sciences
1, Pesek Road, Jurong Island (Singapore)
Fax: (+65) 6316-6182
E-mail: chang_jie@ices.a-star.edu.sg
armando_borgna@ices.a-star.edu.sg

on the application of these types of catalysts in bio-oil upgrading.

Herein, we have systematically screened different carbon-supported metal catalysts for HDO under relatively moderate pressure (4.0 MPa) in continuous packed-bed reactor.[13] To gain an insight into the mechanism of catalytic HDO, guaiacol, a phenolic compound with two types of oxygen-containing functional groups (phenolic and methoxyl groups), was used as a model compound for the second stage of bio-oil upgrading to hydrocarbon fuels. Carbon-supported metal catalysts, such as Pd/C, Cu/C, Ru/C, W/C, Mo/C, Ir/C and Ni/C, were screened in the HDO of guaiacol. The catalyst screening indicated that Ru-based and non-sulfided Mo-based catalysts are the most promising ones. The reaction mechanisms over these two types of catalysts are also discussed.

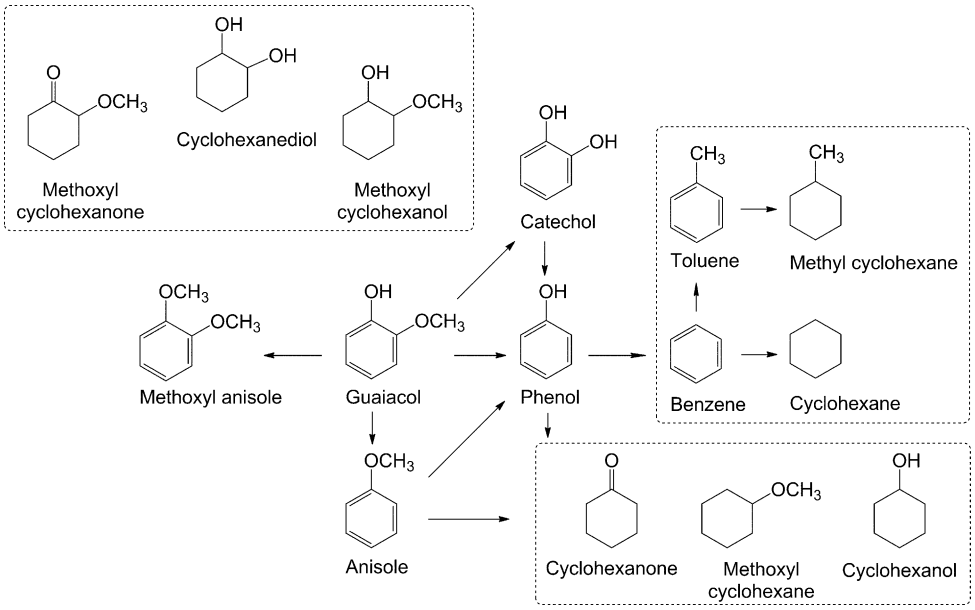

Scheme 1. Reaction network for guaiacol conversion.

Results and Discussion

Catalyst screening for the HDO of guaiacol

The possible reaction network for guaiacol conversion, based on the product distribution observed herein, is shown in Scheme 1. The initial HDO activities over different carbon-supported catalysts are summarised in Table 1. Furthermore, the van Krevelen plot (O/C versus H/C) for the liquid products obtained over different catalysts is shown in Figure 1, which provides a direct evidence of the HDO efficiency. Notably, Ir/C, W/C and Cu/C show negligible activity compared to the thermal conversion of guaiacol (2.4% conversion without catalyst under the same testing conditions). 10Mo/C demonstrates the highest guaiacol conversion and benzene selectivity at 623 K, followed by 1Mo/C and Ru/C. Ru/C provides similar benzene selectivity with 10Mo. However, the saturation of the aromatic ring is also significantly observed and cyclohexanone is the main by-product. This indicates that 10Mo/C has higher H_2 efficiency during the HDO of guaiacol, which is consistent with the observation from the van Krevelen plot (Figure 1). In contrast to the former two catalysts, even though a high guaiacol conversion is obtained over 1Mo/C, phenol is the predominant product, with a selectivity as high as 78.5 wt%. Although Ni/C and Pd/C samples demonstrate catalytic activity in the reaction, both catalysts show high selectivity to products with a saturated C_6 ring, such as cyclohexanol, methoxyl cyclohexane, methoxyl cyclohexanol and methoxyl cyclohexanone; this is in good agree-

Table 1. HDO of guaiacol over carbon-supported catalysts.[a]

Parameter	Ir/C	W/C	Cu/C	Pd/C	Ni/C	Ru/C	1Mo/C	10Mo/C
Metal loading [wt%]	1	1	5	1	5	1	1	10
Conversion of guaiacol [%]	3.2	3.5	3.6	15.5	30.7	34.2	74.1	88.9
Product distribution [wt%]								
cyclohexane	–	–	–	0.7	2.2	3.4	0.3	5.4
benzene	–	–	–	15.3	11.7	34.2	1.5	35.4
toluene	–	–	–	7.3	3.6	2.0	–	–
phenol	–	45.1	33.3	5.8	4.2	19.7	78.5	44.7
anisole	11.2	10.0	3.7	3.2	2.6	4.6	6.2	3.3
methoxyl anisole	40.4	34.0	22.2	4.8	1.5	1.2	3.6	2.3
catechol	48.5	1.9	33.1	4.0	1.8	1.3	2.1	2.5
cyclohexanediol	–	8.6	4.0	0.9	0.3	0.4	5.0	3.4
cyclohexanone	–	–	–	2.6	14.4	21.7	–	–
cyclohexanol	–	–	1.5	16.1	4.3	4.9	–	–
methoxyl cyclohexane	–	–	–	26.7	23.5	6.7	0.1	0.8
methoxyl cyclohexanol	–	–	–	1.5	4.2	–	1.9	1.0
methoxyl cyclohexanone	–	–	–	11.2	25.5	–	–	–

[a] Reaction conditions: 623 K, 4 MPa, $W/F = 0.067$ h, H_2/feed = 20.

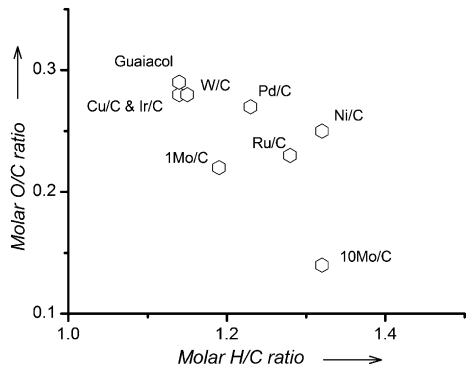

Figure 1. van Krevelen plot for guaiacol conversion over different catalysts. Reaction conditions: 623 K, 4 MPa, $W/F = 0.067$ h, H_2/feed = 20.

ment with a previous work,[11a] which reports that Pd-based catalysts have a low HDO efficiency because they consume more H_2 for aromatic ring saturation rather than for oxygen removal.

According to the screening results, Ru/C and Mo/C catalysts are the most promising catalysts. Therefore, they were further investigated to obtain optimised reaction parameters and a better understanding of the reaction mechanism.

Effect of temperature on the HDO of guaiacol

The effect of the reaction temperature on the conversion of guaiacol and product distribution was investigated over Ru/C, 1Mo/C and 10Mo/C catalysts (Table 2). The conversion of guaiacol reaches 100% over the three catalysts if the reaction temperature is increased from 623 to 673 K at a space–time of 0.067 h. Benzene selectivity over the Ru/C catalyst increases to 69.5 wt% with a dramatic decrease in selectivity to phenol and cyclohexanone. The total selectivity toward aromatic ring saturation decreases from 35.0 to 15.1 wt%. This is consistent with the results reported by Gutierrez et al., which indicate that deoxygenation is favoured over hydrogenation at high temperatures.[14] Over the 10Mo/C catalyst, benzene selectivity also increases to 83.5 wt%. However, the selectivity to benzene over the 1Mo/C sample remains unchanged to approximately 2.0 wt%. The selectivity to cyclohexanediol increases from 5.0 to 14.6%, which indicates the reverse trend of ring saturation activity to Ru/C.

Table 2. Conversion and selectivity over different catalysts.[a]

Parameter	Ru/C	1Mo/C	1Mo/C[b]	10Mo/C	10Mo/C[b]
Conversion [%]	100	98.4	78.7	100	99.4
Selectivity [wt%]					
cyclohexane	7.2	–	–	4.1	–
benzene	69.5	2.4	1.4	83.5	1.6
toluene	–	–	–	–	–
phenol	5.1	76.5	65.5	7.7	71.2
anisole	1.8	3.5	7.2	0.4	7.6
methoxyl anisole	0.3	0.8	12.6	–	7.0
catechol	0.2	0.1	0.9	–	0.6
cyclohexanediol	0.8	14.6	9.4	2.2	9.3
cyclohexanone	–	–	0.5	–	–
cyclohexanol	3.7	0.1	0.1	0.5	0.1
methoxyl cyclohexane	0.8	0.5	–	0.1	–
methoxyl cyclohexanol	8.9	–	–	1.0	–
methoxyl cyclohexanone	0.7	0.4	0.9	–	–

[a] Reaction conditions: 673 K, 4 MPa, $W/F = 0.067$ h, H_2/feed = 20. [b] Mo catalysts without pre-reduction.

Effect of space–time on the HDO of guaiacol

The effect of space–time on product distribution over different catalysts is shown in Figure 2. Because of the complexity of product composition, only the selectivity to the main products is shown. The selectivity changes with space–time over the Ru/C sample. If the space–time is less than 0.0087 h, catechol is the dominant product over the Ru/C catalyst. At higher contact times, the selectivity to catechol decreases monotonically whereas the selectivity to phenol reaches the maximum value of 49 wt% at 0.017 h. If the space–time is more than 0.033 h, the benzene yield increases significantly and becomes the dominant product at 0.067 h. The evolution of product distribution suggests that catechol is the primary intermediate, which is formed via the demethylation of the methoxyl group over Ru/C catalysts.

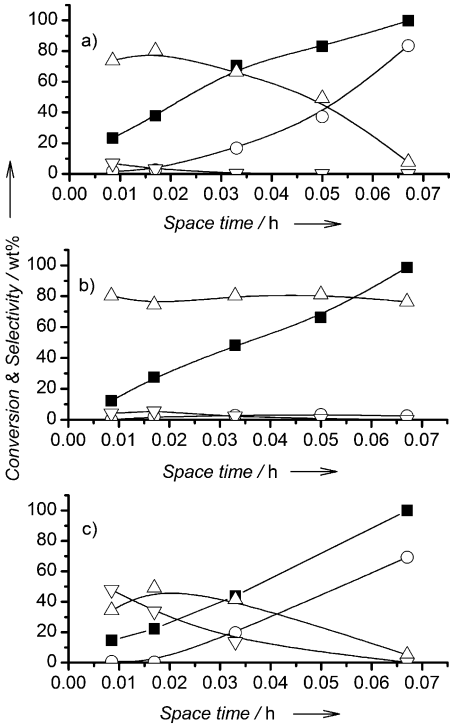

Figure 2. Product distribution over a) 10Mo/C, b) 1Mo/C, and c) Ru/C catalysts. Reaction conditions: 623 K, 4 MPa, $W/F = 0.067$ h, H_2/feed = 20. Guaiacol conversion (■), benzene selectivity (○), phenol selectivity (△), catechol selectivity (□).

However, over both 10Mo/C and 1Mo/C catalysts, phenol is detected as the dominant intermediate instead of catechol. Only 6.8 wt% of catechol is detected at a space–time of 0.0087 h over the 10Mo/C catalyst. Catechol selectivity decreases with increasing space–time. In contrast, phenol selectivity is as high as 73.8 wt% at 0.0087 h and decreases slowly while benzene production increases. The 1Mo/C catalyst shows an even higher phenol yield. Approximately 80 wt% of phenol selectivity is observed, which is constant in the entire range of space–time, although the conversion level of guaiacol changes from 12.2 to 98.5% with the change in space–time.

The van Krevelen plot shown in Figure 3 indicates that both Ru/C and 10Mo/C catalysts can hydrodeoxygenate guaiacol to fuel-like products with an O/C molar ratio lower than 0.05. In addition, the 10Mo/C catalyst provides good H_2 efficiency whereas the Ru/C catalyst produces more saturated C_6 ring if guaiacol conversion approaches 100%. Over the 1Mo/C catalyst, the O-containing groups of guaiacol cannot be removed

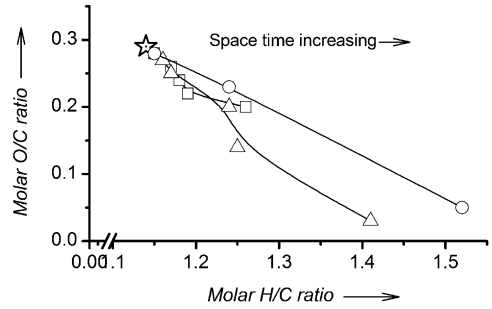

Figure 3. van Krevelen plot over catalysts 10Mo/C (△), 1Mo/C (□), and Ru/C (○). Reaction conditions: 623 K, 4 MPa, $W/F = 0.067$ h, H_2/feed = 20. The input of guaiacol feedstock is marked by ☆.

completely and phenol is the dominant product if guaiacol conversion approaches 100% at a space–time of 0.068 h.

Catalyst characterisation

According to the catalytic tests over Ru- and Mo-based catalysts, the catalytic behaviour is significantly different over these samples. To identify the nature of active phases in Ru/C and Mo/C catalysts, temperature programmed reduction (TPR), XRD and XPS characterisations were performed.

The TPR profiles illustrated in Figure 4 show a sharp H_2 consumption peak and a weak broad peak for the Ru-based sample at 394 and 495 K, respectively. This indicates that RuO_x is reduced to Ru^0.[16] The TPR profile of carbon-supported Mo

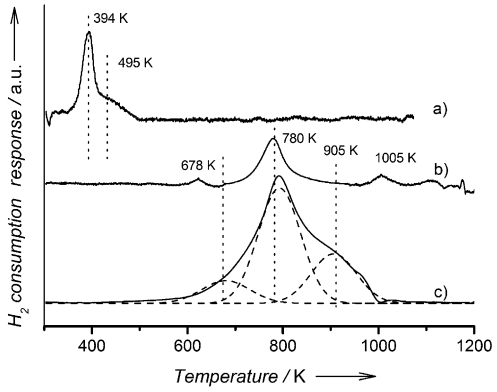

Figure 4. Temperature programmed reduction profiles of a) Ru/C, b) 1Mo/C and c) 10Mo/C catalysts.

catalysts shows mainly three H_2 consumption peaks appearing at 680, 780 and approximately 900 K, marked by dotted lines. It was suggested that the first two peaks, at temperatures lower than 800 K, may be attributed to the reduction of Mo species with octahedral coordination while the H_2 consumption peak at approximately 800 K may be attributed to the reduction of tetrahedrally coordinated Mo species (Mo-T).[15] Peak III can be attributed to the carburisation and deep reduction[17] of Mo species over carbon surfaces. The deconvolution of TPR profiles shows that the content of more refractory Mo-T species, which is represented by the area ratio of peak II/peak I, is higher for the 1Mo/C catalyst than for the 10Mo/C catalyst (35.6 vs. 4.5, respectively). Furthermore, the area ratio of peak III/(peak I + peak II) for the 1Mo/C catalyst is much smaller than that of the 10Mo/C catalyst (0.08 vs. 0.37, respectively). It indicates that the dominant molybdenum oxide in the 1 wt% Mo catalyst is Mo-T, which is more difficult to be reduced.

Because of the low loadings of Ru/C and 1Mo/C samples, the active phases are well dispersed over the carbon surface and crystallite sizes measured from CO chemisorption are 2.3 and 2.5 nm, respectively. Thus, only two broad and not well-defined peaks, which can be assigned to activated carbon, were observed for these samples. XRD was used only to explore the phase change during H_2 reduction for the 10Mo/C catalyst. The XRD patterns for the fresh and reduced 10Mo/C catalysts are shown in Figure 5. The only Mo species observed in the fresh 10Mo/C catalyst is MoO_3, with diffraction peaks at

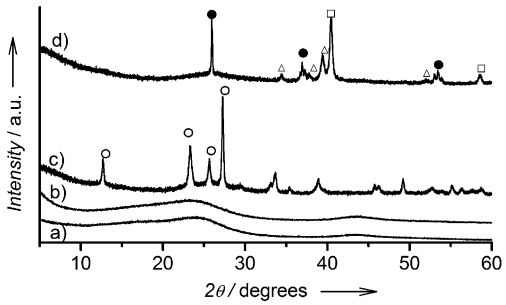

Figure 5. XRD patterns of a) fresh Ru/C, b) fresh 1Mo/C, c) fresh 10Mo/C and d) reduced 10Mo/C catalysts at 973 K. MoO_3 (○), MoO_2 (●), β-Mo_2C (△) and metal Mo^0 (□).

23.3, 25.7, 27.3, 33.7 and 38.9°. After reduction in flowing H_2 at 973 K, three Mo phases can be identified on the basis of JCPDS database: MoO_2 (25.9, 36.9 and 53.5°), beta-Mo_2C (34.5, 38.0 and 39.6°) and metallic Mo^0 (40.4 and 58.7°). The formation of metallic Mo^0 during the reduction of Mo/C catalysts was observed by Li.[17c] It was reported that metallic Mo^0 can be formed over Mo/C catalysts if the reduction temperature is lower than 973 K. If the temperature is increased, Mo^0 reacts with the carbon support and forms beta-Mo_2C. Furthermore, Mo^0 species can be carburised easily by carbon-containing feedstock at approximately 510–570 K at the initial reaction time.[17a,b,d]

The Mo 3d X-ray photoelectron spectra of 1Mo/C and 10Mo/C catalysts are shown in Figure 6. The deconvoluted XPS results, providing the distribution of Mo species, are summarized in Table 3. Notably, the XPS spectra of the as-prepared 1Mo/C and 10Mo/C catalysts are similar, which shows only one doublet located at 232.4 eV and thus indicates the presence of only Mo^{6+} species (MoO_3); this is in good agreement with the XRD results. The peak deconvolution of the reduced 1Mo/C catalyst reveals two doublets. The new doublet with a Mo $3d_{5/2}$ binding energy of 229.4 eV can be assigned to the formation of Mo^{4+} during H_2 reduction.[18] The atomic percentage of MoO_3 and MoO_2 are 76.6 and 23.4%, respectively. Although

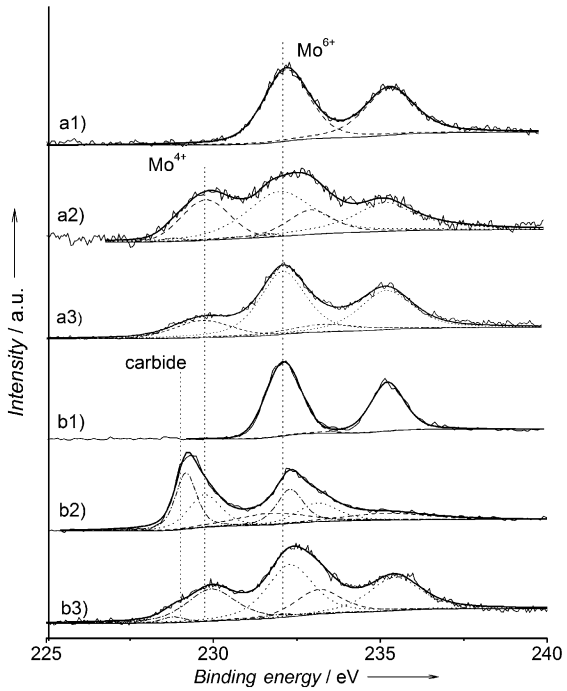

Figure 6. Mo 3d XPS spectra of 1Mo/C and 10Mo/C catalysts: a1) fresh 1Mo/C, a2) reduced 1Mo/C, a3) spent 1Mo/C, b1) fresh 10Mo/C, b2) reduced 10Mo/C and b3) spent 10Mo/C.

Table 3. Chemical states of reduced Mo-based catalysts derived from the peak deconvolution of XPS curves.

Mo species	XPS peaks		Relative percentage [%]			
	Mo $3d_{3/2}$	Mo $3d_{5/2}$	1Mo/C	10Mo/C	1Mo/C[a]	10Mo/C[a]
Mo^{6+}	235.6	232.7	76.6	25.6	65.4	56.8
Mo^{4+}	233.0	229.4	23.4	33.9	34.6	43.3
Carbide	232.0	228.6	–	40.5	–	–

[a] Spent Mo-based catalysts (without H_2 reduction before reaction).

two Mo species are detected on the low Mo loading catalyst, the XPS spectrum of the reduced 10Mo/C catalyst reveals the existence of three doublets. The Mo $3d_{5/2}$ peak located at 229.4 eV is assigned to Mo^{4+} species of MoO_2, whereas the doublet at 228.6 eV is assigned to a molybdenum carbide phase, which is in good agreement with the binding energy reported in the literature on carbide species.[19] The corresponding atomic percentage of MoO_2 and Mo_2C are 33.9 and 40.5 %, respectively. The XPS surface analysis reveals significant differences between both Mo catalysts. Although oxide species are detected only in the 1Mo/C sample, molybdenum carbide is the dominant species in the 10Mo/C catalyst.

To clarify the relationship between the chemical states of Mo species and the catalytic performance, catalytic tests using unreduced Mo samples were performed (Table 2, columns 3 and 5). Phenol is the main product over both catalysts. Therefore, the unreduced catalysts demonstrate a product distribution similar to the one obtained on the reduced 1Mo/C catalyst. The spent catalysts were analysed further by using XPS. Molybdenum carbides cannot be detected, whereas Mo^{6+} and Mo^{4+} are the dominant species over both catalysts (Table 3, columns 3 and 4). These results suggest that MoO_x is the active phase for the conversion of guaiacol into phenol. Phenol could be further converted into benzene on carbide sites.

Additional catalytic tests using intermediate reaction products

Additional catalytic tests using intermediate reaction products—anisole and catechol—as feedstock were performed over Ru/C and Mo/C catalysts. Owing to the high boiling point of catechol, it was fed as a 20 wt% solution in guaiacol.

Anisole can be readily converted over the three catalysts (Table 4). Ru/C and 10Mo/C catalysts demonstrate a product distribution similar to that for the HDO of guaiacol (Table 2). The cleavage of the anisole aryl–OCH_3 bond was studied by Afifi et al.[20] The cleavage of the O–CH_3 bond [Eq. (1)] is energetically favoured in comparison to that of the aryl–O bond [Eq. (2)]. Over metal catalysts, a weak coordinative bond can be formed between the methoxyl group and the active site through the free electron pairs of the oxygen atom. Then, the O–CH_3 bond dissociates homolytically and forms phenoxide and methyl radicals, which are hydrogenated to phenol and methane.[21] Thus, catechol was observed as the primary inter-

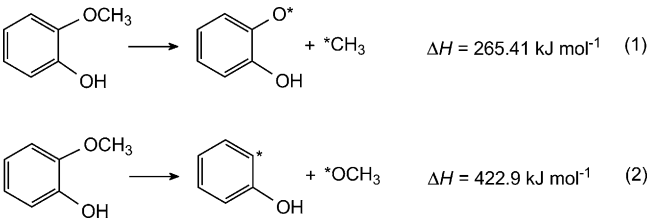

Table 4. Conversion and selectivity over different catalysts in anisole and catechol HDO reactions.[a]

Parameter	Anisole			20% catechol in guaiacol		
	Ru/C	1Mo/C	10Mo/C	Ru/C	1Mo/C	10Mo/C
Conversion [%]	52.3[b]	19.2[b]	19.4[b]	85.5[c] 95.9[d]	27.3[c] 44.1[d]	47.5[c] 67.9[d]
Selectivity [wt%]						
cyclohexane	1.1	–	–	8.7	0.1	–
benzene	77.5	74.9	84.4	42.4	1.0	29.0
toluene	–	1.4	5.7	1.0	1.1	5.9
phenol	3.4	20.6	8.1	31.6	76.5	52.8
anisole	–	–	–	3.4	3.0	1.6
methoxyl anisole		–	–	0.1	0.8	1.0
cyclohexanediol	–	–	–	1.8	11.1	8.2
cyclohexanone	5.1	1.2	–	3.6	0.2	0.5
cyclohexanol	12.9	0.9	–	6.2	5.7	–
methoxyl cyclohexane	–	1.0	1.9	0.8	0.2	–
methoxyl cyclohexanol	–	–	–	–	–	–
methoxyl cyclohexanone	–	–	–	0.2	0.1	–

[a] Reaction conditions: 673 K, 4 MPa, $W/F = 0.067$ h and H_2/feed = 20; [b] Conversion of anisole; [c] Conversion of guaiacol; [d] Conversion of catechol.

mediate of the HDO of guaiacol over the Ru/C catalyst because it is the preferred reaction pathway from an energetic point of view. Therefore, the HDO of guaiacol over the Ru/C catalyst should follow the reaction pathway suggested by Delmon and Laurent (Scheme 2).[22]

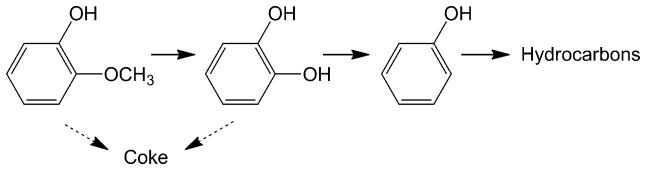

Scheme 2. Mechanism of the HDO of guaiacol proposed by Delmon and Laurent.[22]

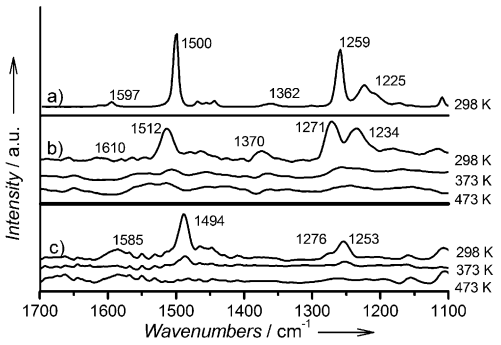

Figure 7. FTIR spectra of guaiacol: a) guaiacol, b) guaiacol adsorbed on MoO_3 and c) guaiacol adsorbed on reduced MoO_3.

However, this mechanism cannot explain the product distribution obtained over the 1Mo/C catalyst during guaiacol experiments (Table 2), in which phenol is the main product with a selectivity of approximately 80%. Similarly, a high phenol selectivity during the HDO of guaiacol over carbon-supported CoMo sulfide catalysts was reported by Delmon et al.[23] This was explained assuming that the direct hydrogenolysis of the aryl–OCH_3 bond may occur on metal sulfides; however, no clear evidence was provided. Notably, over the 1Mo/C catalyst, in which MoO_x is the dominant species, benzene is formed as the main product during anisole experiments. This indicates that demethoxylation rather than demethylation is the main reaction pathway over MoO_x. This finding is also supported by our previous guaiacol experiments, which shows that a minor benzene yield is obtained over Mo-based catalysts without carbide phases. No further HDO of phenol occurs over MoO_x species, as clearly indicated in Table 2.

Co-feeding catechol with guaiacol significantly inhibits guaiacol conversion while a higher phenol/benzene ratio is observed. This may be attributed to the competitive adsorption between catechol and guaiacol, particularly on Mo-based catalysts. It is known that Mo^{6+} ions can react with catechol to form a stable complex.[24] These results also suggest a strong interaction between catechol and other $Mo^{\delta+}$ ions, as indicated by the decrease in the reaction rate in catechol co-feeding experiments. Furthermore, the increase in phenol selectivity on the 10Mo/C catalyst, in which carbides are the dominant surface species and have less effect on catechol competitive adsorption, indicates that although catechol can also be converted, without the synergistic effects of MoO_x sites its oxygen-removal efficiency is significantly reduced. Thus, the direct cleavage of the aryl–OCH_3 bond resulting in phenol formation seems to be the predominant pathway over MoO_x sites to form catechol as an intermediate in comparison to the demethylation route.

FTIR study of adsorbed guaiacol

The typical FTIR spectrum of guaiacol between 1100 and 1700 cm^{-1} as a reference is shown in Figure 7a. Over MoO_3, the aromatic C=C band positions shift to higher wavenumbers, 1610 and 1512 cm^{-1}, respectively. In addition, significant contribution from δ(OH) vibrations, shifting from 1362 to 1370 cm^{-1}, is observed. It could be attributed to interactions through hydrogen bonds. Over reduced MoO_3, the main bands for aromatic ring vibration at 1597 and 1501 cm^{-1} shift to lower wavenumbers, 1585 and 1494 cm^{-1}, respectively. This indicates the presence of an electrodonation effect of the oxygen atom on the aromatic ring over molybdenum oxide with lower oxidation states. In addition, the δ(OH) vibration at 1362 cm^{-1} is no longer detected while the other bands are still quite strong. This could indicate the removal of –OH groups and the formation of phenate species. The intensity of the band at 1253 cm^{-1}, assigned to the asymmetric C–O–C bond, decreases significantly, whereas the band at 1225 cm^{-1}, assigned to the C–OCH_3 bond, disappears and a new band at 1276 cm^{-1} is detected, which could be attributed to the interaction between methoxyl groups and MoO_x. An IR spectroscopic study on the adsorption and activation of guaiacol over oxides was reported by Popov et al.[25] The peaks at approximately 1330 and 1225 cm^{-1} were assigned to aryl–OH and aryl–OCH_3 bonds, and both are eliminated at a high temperature (673 K). Therefore, the formation of a doubly-anchored guaiacol surface species was suggested over oxides with Lewis sites. This is consistent with our observations over MoO_x, which indicates that a doubly-anchored intermediate could be formed.

Furthermore, a redox mechanism of guaiacol deoxygenation via doubly-anchored guaiacol intermediate over Al_2O_3-supported vanadium oxide catalysts was proposed by Filley and Roth.[26] In this mechanism, methyl catechol is formed firstly over the Lewis acid sites of the Al_2O_3 support. Then, oxygen species available on the neighbour site of phenolic groups are subtracted by V^{3+} to restore the V^{5+} sites while hydrogen is transferred to an aryl carbon to break the aryl–O bond, which yields cresol.

Therefore, for Mo/C catalysts, an activation mechanism of guaiacol via a doubly-anchored surface intermediate over residual MoO_3 (Scheme 3) could be envisaged. In contrast to the case of vanadium oxide, no significant production of alkylation products, such as methyl anisole and cresol, was detected over our Mo/C catalysts, owing probably to the lack of acidity of the carbon surface. However, methanol is observed in the

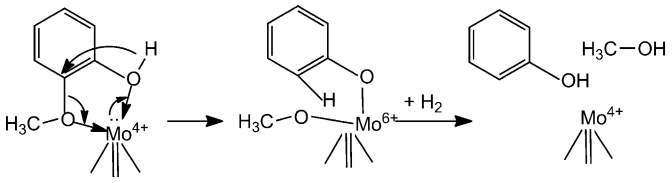

Scheme 3. Doubly-anchored activation mechanism of the HDO of guaiacol over MoO_x.

liquid product obtained if Mo-based catalysts are used. This indicates that the cleavage of the aryl–OCH_3 bond and consecutive methylation before activation is not required, at least over carbon-supported Mo catalysts. It could be speculated that guaiacol adsorbs molecularly on Mo^{4+} sites to form a doubly-chelated phenate intermediate directly instead of getting converted into methyl catechol first. Thus, the oxygen atom is captured from guaiacol and Mo site is oxidised to Mo^{6+}. Then, hydrogenation occurs, which leads to the formation of reaction products and reduces Mo^{6+} species to Mo^{4+}, and this complete the catalytic cycle.

Therefore, the reaction mechanism of the HDO of guaiacol over Mo/C catalysts could be envisaged. In this mechanism, partially reduced MoO_x species act as active sites for the direct demethoxylation of guaiacol to form phenol. The resulting phenol can be deoxygenated further on adjacent carbide sites to produce benzene. However, because catechol adsorbs more strongly on MoO_x, the demethoxylation route is partially blocked if catechol is co-fed. Thus, demethylation to catechol followed by deoxygenation to phenol and then to benzene becomes the main pathway over carbide sites. In addition, owing to the competitive catechol adsorption on carbide sites, the phenol HDO reaction rate is affected, which results in lower guaiacol conversion and higher phenol selectivity in co-feeding experiments over the 10Mo/C catalyst.

Catalyst deactivation

The deactivation behaviour was evaluated for Ru/C, 1Mo/C and 10Mo/C catalysts during 6 h of time on stream (Figure 8). Two types of deactivation patterns are observed. 1Mo/C and 10Mo/C catalysts deactivate monotonically during the entire time on stream, whereas the deactivation of the Ru/C catalyst shows a two-stage deactivation regime: 1) a sharp decrease in activity is observed at the beginning of the reaction and 2) a slow deactivation occurs, which reaches a pseudo-steady-state conversion level. The most possible cause for deactivation is coking, as reported by Delmon and Laurent.[22] Some tar-like heavy products were also observed over the inert supporting materials (e.g., quartz wool and glass bead) in the reactor. However, there is not enough direct evidence to attribute the deactivation exclusively to coke formation because a carbon-based support was used in this work. Further investigations are necessary to explore deactivation mechanisms over Ru/C and Mo/C catalysts.

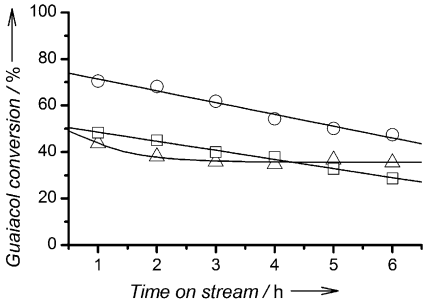

Figure 8. Catalyst deactivation during the HDO of guaiacol over 10Mo/C (○), 1Mo/C (□) and Ru/C (△) catalysts. Reaction conditions: 673 K, 4.0 MPa, $W/F = 0.033$ h, H_2/feed = 20.

Conclusions

The hydrodeoxygenation of guaiacol, a model reaction for bio-oil upgrading to produce renewable hydrocarbon-like fuels, was investigated. The reaction occurs readily over carbon-supported Ru and Mo catalysts under moderate pressure (4.0 MPa) and yields benzene and phenol as dominant products. The product distribution indicates that the conversion of guaiacol occurs through different reaction pathways over Mo/C and Ru/C catalysts. Over MoO_x sites, guaiacol could be converted directly into phenol via the formation of a doubly-anchored intermediate, followed by the direct removal of the methoxyl group. In contrast, the formation of phenol over Ru/C catalysts occurs preferentially via the cleavage of the CH_3–O bond of the methoxyl group and catechol is formed as an intermediate product. Metallic ruthenium and molybdenum carbides are the active phases for deep deoxygenation to benzene, which results in complete oxygen removal. Significantly different deactivation behaviour was observed over Mo-based and Ru-based catalysts. While the Mo-based catalyst deactivates monotonically, the Ru-based catalyst shows a fast initial deactivation, then reaches a pseudo-steady-state residual activity.

Experimental Section

Catalyst preparation

Carbon-supported metal catalysts (Pd, Cu, Ru, Ir, Ni and Mo) were prepared through incipient wetness impregnation. Before metal impregnation, a commercial activated carbon used as a support (NORIT R 3 EXTRA) was grinded and sieved into 20–40 mesh. Then, the carbon support was treated with nitric acid by using a refluxing method at 353 K overnight. Next, it was washed with deionised water and dried at 383 K. Metal impregnation was performed by using the aqueous solution of the active metal salts at appropriate concentrations to yield the desired metal loadings. Palladium(II) nitrate, copper(II) nitrate trihydrate, ruthenium(III) acetylacetonate, iridium(III) chloride hydrate, nickel(II) nitrate hexahydrate and ammonium heptamolybdate tetrahydrate (supplied by Strem Chemicals Inc.) were used as metal precursors for Pd, Cu, Ru, Ir, Ni and Mo, respectively. After impregnation, the catalysts were kept at RT for 4 h and then dried at 373 K overnight. Finally, the resulting catalysts were calcined at 673 K in flowing N_2 for 5 h.

Catalytic activity and control reactions

The catalytic activity measurements were performed in a stainless steel fixed-bed tubular reactor (outer diameter = 0.5 in.). The reaction was performed at temperatures ranging from 623 to 673 K and 4 MPa. A H_2/guaiacol molar ratio of 20 was used in all experiments. The space–time, expressed as *W/F*, in which *W* is the mass of the catalyst (g) and *F* is the feed flow rate (g h^{-1}), was varied systematically by changing either the catalyst loading or the feed flow rate. Before the reaction, the catalyst was reduced in situ in flowing H_2 for 1 h at 673 K and 4.0 MPa, except for Mo/C catalysts, which were reduced at 973 K. After reduction, the reactor was cooled to the reaction temperature. Subsequently, guaiacol was fed into the reactor. The reaction products were condensed in a sample cylinder and collected within 1 h intervals. The collected liquid samples were weighed and analysed with an Agilent 6890 gas chromatograph equipped with an HP-5 column. For all experiments reported here, the average value of the mass balance, calculated as the ratio between the weight of the condensed liquid product and the weight of the reactant fed into the reactor, was 85.6%. An Agilent 6890 gas chromatograph was used for product identification. Product identification was verified by using standards. Moreover, an element-sensitive GC analysis of the liquid products was also performed with an Agilent 6890 gas chromatograph equipped with a JAS atomic emission detector.

Conversion and product selectivity were calculated by using Equations (3 a, b):

$$X(\%) = \frac{1 - C_G W_{lp}}{W_i} \times 100 \quad (3a)$$

$$S_j(\%) = \frac{C_j}{\sum C_j} \times 100 \quad (3b)$$

in which C_j is the concentration of the reaction product j measured by GC, C_G is the guaiacol concentration in the liquid product, W_i is the weight of the reactant fed during the sampling interval and W_{lp} is the weight of the liquid product.

Control reactions for guaiacol and anisole were performed over activated carbon under common conditions used in catalyst evaluations (673 K, 4.0 MPa, $W/F = 0.067$ h). The conversion values were 15.1 and 4.6% for guaiacol and anisole, respectively. Catechol (33.6%) and phenol (15.5%) were observed as the dominant products in the guaiacol control experiment, whereas in the anisole control reaction, phenol (54.7%) was the main product.

Catalyst characterisation

Catalyst reducibility was determined by using the TPR technique. TPR measurements were performed with a Thermo Scientific TPROD 1100. The calcined catalyst (50 mg), thermally treated under Ar atmosphere at 773 K to remove water and other contaminants, was heated from 303 to 1123 K (heating rate: 10 K min^{-1}) under a 5% H_2/Ar mixture (flow rate: 50 mL min^{-1}) and kept at 1123 K for 15 min while the hydrogen consumption was monitored continuously.

XPS was used to investigate the surface composition of the catalyst. The XPS spectra were recorded on a Thermo ESCALAB 250 spectrometer using AlK_α radiation ($h\nu = 1486.6$ eV). Measurements were performed with 20 eV pass energy, 0.1 eV step size and 0.1 s dwelling time. Energy correction was performed by using the C 1s peak of adventitious carbon at 284.5 eV as a reference. Reduced samples were treated ex situ in flowing H_2 at 973 K and then passivated. With minimal exposure to air, samples were loaded in the XPS reactor cell located inside the XPS pre-chamber and re-reduced in flowing H_2 at 773 K. After re-reduction and evacuation, samples were transferred to the main XPS chamber and XPS spectra were recorded.

Powder XRD measurements were performed with a Bruker D8 Advance X-ray diffractometer equipped with a RINT2000 wide-angle goniometer. Diffraction patterns were recorded within the range of $2\theta = 5–70^\circ$ (step size: 0.02°) by using CuK_α radiation and a power of 40 kV × 40 mA. Reduced samples were treated ex situ in flowing H_2 at 973 K and then passivated before recording XRD patterns.

The FTIR spectra were recorded with a Bio-Rad Excalibur Series FTS 3000 system equipped with a mercury cadmium telluride detector and a high-temperature DRIFT cell fitted with KBr windows. In a typical experiment, the sample was treated initially at 673 K for 2 h in flowing He (UHP, 99.999%; flow rate: 20 mL min^{-1}). The spectra recorded under He flow at ambient temperature were used as reference. Next, guaiacol was introduced by dropping the liquid (20 μL) on the powder sample. Then, the cell was evacuated at 30 mbar (3 kPa) to remove excess guaiacol until the spectra became constant. The spectra were acquired with a resolution of 4 cm^{-1}. Typically, 256 scans were recorded, averaged and transformed by using the Kubelka–Munk method, and the spectra recorded before introducing guaiacol was used as reference.

Acknowledgements

*This work has been financially supported by the Thematic Strategic Research Program (grant no. 0921390037) from the Science and Engineering Research Council (SERC), Agency for Science, Technology, and Research (A*STAR), Singapore.*

Keywords: bio-oil · guaiacol · hydrodeoxygenation · molybdenum · ruthenium

[1] a) C. Amen-Chen, H. Pakdel, C. Roy, *Biomass Bioenergy* **2001**, *79*, 277–287; b) E. Berl, *Sciences* **1944**, *99*, 309–330; c) D. Mohan, C. Pittman, Jr., P. Steele, *Energy Fuels* **2006**, *20*, 848–889.

[2] a) Y. Sheu, R. Anthony, E. Soltes, *Fuel Process. Technol.* **1988**, *19*, 31–50; b) S. Czernik, A. Bridgwater, *Energy Fuels* **2004**, *18*, 590–598; c) D. Resasco, S. Crossely, *AIChE J.* **2009**, *55*, 1082–1089.

[3] a) M. Fatih Demirbas, *Appl. Energy* **2009**, *86*, S151–S161; b) L. Rollmann, *J. Catal.* **1977**, *46*, 243–252.

[4] a) I. Graça, F. Ribeiro, H. Cerqueira, Y. Lam, M. Almeida, *Appl. Catal. B* **2009**, *90*, 556–563; b) E. Furimsky, *Appl. Catal. A* **2000**, *199*, 147–190; c) D. Elliott, *Energy Fuels* **2007**, *21*, 1792–1815; d) A. Ausavasukhi, T. Sooknoi, D. Resasco, *J. Catal.* **2009**, *268*, 68–78.

[5] a) E. Laurent, B. Delmon, *Appl. Catal. A* **1994**, *109*, 77–96; b) Y. Romero, F. Richard, S. Brunet, *Appl. Catal. B* **2010**, *98*, 213–223; c) R. Nava, B. Pawelec, P. Castaño, M. Álvarez-Galván, C. Loricera, J. Fierro, *Appl. Catal. B* **2009**, *92*, 154–167; d) W. Baldauf, U. Balfanz, M. Rupp, *Biomass Bioenergy* **1994**, *7*, 237–244.

[6] a) S. Zhang, *Energy Sources* **2003**, *25*, 57–65; b) M. Samolada, W. Baldauf, I. Vasalos, *Fuel* **1998**, *77*, 1667–1675.

[7] A. Oasmaa, E. Leppämmäki, P. Koponen, J. Levander, E. Tapola, "Application of Standard Fuel Oil Analyses", VTT Publication 306, **1997**.

[8] C. Fisk, T. Morgan, Y. Ji, M. Crocker, C. Crofcheck, S. Lewis, *Appl. Catal. A* **2009**, *358*, 150–156.

[9] D. Elliott, T. Hart, *Energy Fuels* **2009**, *23*, 631–637.

[10] A. Centeno, A. David, C. Vanbellinghen, R. Maggi, B. Delmon, *Developments in Thermochemical Biomass Conversion* (Eds.: A. V. Bridegwater, D. G. Boocock), Blackie Academic and Scientific, London, UK, **1997**, pp. 589 – 601.
[11] a) J. Wildschut, F. Mahfud, R. Venderbosch, H. Heeres, *Ind. Eng. Chem. Res.* **2009**, *48*, 10324 – 10334; b) C. Zhao, Y. Kou, A. Lemonidou, X. Li, J. Lercher, *Angew. Chem.* **2009**, *121*, 4047 – 4050; *Angew. Chem. Int. Ed.* **2009**, *48*, 3987 – 3990.
[12] a) L.Thompson, P. Savage, D. Briggs, *Novel catalysts for upgrading coal-derived liquids*. Final technical progress report, DOE/PC/92537-T12, **1995**; b) T. Xiao, A. York, K. Coleman, J. Claridge, J. Sloan, J. Charnock, M. Green, *J. Mater. Chem.* **2001**, *11*, 3094 – 3098.
[13] Q. Bu, H. Lei, A. Zacher, L. Wang, S. Ren, J. Liang, Y. Wei, Y. Liu, J. Tang, Q. Zhang, R. Ruan, Biores. Tech. **2012**, *124*, 470–477.
[14] A. Gutierrez, R. Kaila, M. Honkela, R. Slioor, A. Krause, *Catal. Today* **2009**, *147*, 239 – 246.
[15] a) L. Feng, X. Li, D. Dadyburjor, E. Kugler, *J. Catal.* **2000**, *190*, 1 – 3; b) T. Bhaskar, K. Reddy, C. Kumar, M. Murthy, K. Chary, *Appl. Catal. A* **2001**, *211*, 189 – 201.
[16] P. Koopman, A. Kieboom, H. Bekkum, *J. Catal.* **1981**, *69*, 172.
[17] a) D. Mordenti, D. Brodzki, G. Djega-Mariadassou, *J. Solid State Chem.* **1998**, *141*, 114; b) E. Kugler, C. Clark, J. Wright, D. Dadyburjor, J. Hanson, Z. Song, T. Cai, J. Hrbek, *Top. Catal.* **2006**, *39*, 257; c) X. Li, M. Ding, X. Bao, *Chin. J. Catal.* **2008**, *29*, 884; d) J. Lee, M. Boudart, *Catal. Lett.* **1993**, *20*, 97.
[18] A. Yong, H. Borg, L. Ijzendoorn, W. Soundant, V. Beer, J. Veen, J. Niemantsverdriet, *J. Phys. Chem.* **1993**, *97*, 6477 – 6483.
[19] a) R. Barthos, A. Széchenyi, Á. Koós, F. Solymosi, *Appl. Catal. A* **2007**, *327*, 95 – 105; b) L. Leclercq, M. Provost, H. Pastor, J. Grimblot, A. Hardy, L. Gengembre, G. Leclercq, *J. Catal.* **1989**, *117*, 371 – 383.
[20] A. Afifi, J. Hindermann, E. Chornet, R. Overend, *Fuel* **1989**, *68*, 498.
[21] J. Bredenberg, M. Huuska, J. Raty, M. Koiwio, *J. Catal.* **1982**, *77*, 242.
[22] E. Laurent, B. Delmon, *Appl. Catal.* **1994**, *109*, 97.
[23] A. Centeno, E. Laurent, B. Delmon, *J. Catal.* **1995**, *154*, 288.
[24] K. Kustin, S. Liu, *J. Am. Chem. Soc.* **1973**, *95*, 2487.
[25] A. Popov, E. Kondratieva, J. Goupil, L. Mariey, P. Bazin, J. Gilson, A. Travert, F. Mauge, *J. Phys. Chem. C* **2010**, *114*, 15661.
[26] C. R. Filley, C. Roth, *J. Mol. Catal. A-Chem.* **1999**, *139*, 245 – 252.

Received: February 4, 2013
Revised: March 22, 2013
Published online on ■■ ■■, 0000